LAWRENCE
LIVERMORE
NATIONAL
LABORATORY

LLNL-JRNL-652799

Computational Investigation of Electron Small Polarons in Alpha-MoO3

H. Ding, H. Lin, B. Sadigh, F. Zhou, V. Ozolins, M. Asta

April 8, 2014

Journal Of Physical Chemistry C

Disclaimer

Computational Investigation of Electron Small Polarons in α-MoO_3

Hong Ding,[*,†] Hao Lin,[‡] Babak Sadigh,[¶] Fei Zhou,[¶] Vidvuds Ozoliņš,[‡] and Mark Asta[†]

Department of Materials Science and Engineering, University of California, Berkeley, CA, USA, Department of Materials Science and Engineering, University of California, Los Angeles, CA, USA, and Lawrence Livermore National Laboratory, Livermore, CA, USA

E-mail: hongding@berkeley.edu

[*]To whom correspondence should be addressed
[†]Department of Materials Science and Engineering, University of California, Berkeley, CA, USA
[‡]Department of Materials Science and Engineering, University of California, Los Angeles, CA, USA
[¶]Lawrence Livermore National Laboratory, Livermore, CA, USA

Abstract

The properties of electron small polarons in α-MoO_3 are investigated computationally employing density-functional-theory with Hubbard-U corrections (DFT+U) and hybrid functionals (HSE06). These methods are used to compute the electronic and atomic structures of polarons localized on Mo ions, the barrier for adiabatic polaron hopping, and the magnitude of the binding energy with intercalated Li ions. The calculations establish a pronounced anisotropy in polaron mobilities, both within the bilayer sheets and across the van der Waals (vdW) gaps characteristic of the α-MoO_3 structure. The lowest and highest energy barriers are found for hopping within the same bilayer plane and across the vdW gap, respectively. The binding energies between polarons and intercalated Li ions are calculated in supercells with composition $Li_{0.028}MoO_3$, yielding values of 0.34 eV when Li ions are located in the one-dimensional channels within the bilayer sheets, and 0.26 eV when Li resides in the two-dimensional interlayer van der Waals gaps.

Introduction

Due to its attractive electrochemical properties and layered crystal structure, α-MoO_3 has been investigated extensively as a Li-ion intercalation compound for energy storage applications. Recently, the interest in this compound for such applications has expanded due to the development of synthesis techniques for producing nanoscale and mesoporous forms of the material .[1–5] The high specific area achievable through such synthesis routes has led to enhanced performance in battery applications, as well as recent demonstrations of the successful use of this compound as an electrode material for electrochemical pseudocapacitors .[6,7] For such applications, the performance of α-MoO_3 is limited by its intrinsically low electronic conductivity (σ_e), and a number of different strategies have been developed for improving this property, e.g., through oxygen reduction,[8,9] extrinsic doping,[10,11] and the development of composite material architectures.[12,13] To guide such efforts, an expanded understanding of the intrinsic mechanisms underlying electronic transport in α-MoO_3, and the ways they can be influenced by variations in composition and structure, is

desirable.

Depending on the synthesis procedure, intrinsic room-temperature electronic conductivities in α-MoO_3 have been reported to vary over several orders of magnitude, from values of $\sigma_e \approx 10^{-10}$ to $\sigma_e \approx 10^{-4}$ S·cm^{-1}.[3,14,15] Similarly large variations in σ_e can be effected through extrinsic doping. For example, in a recent investigation by Berthumeyrie *et al.*,[16] dielectric spectroscopy techniques were used to study variations in the mechanisms underlying electronic transport in Li_xMoO_3 as a function of the Li content x. At room-temperature the measured values of σ_e were reported to vary from 10^{-10} to 0.46 S·cm^{-1} as x ranged from 0 to 0.45 in "classical powder" (CP) samples consisting of micron-scale particles, and from 3×10^{-6} S·cm^{-1} for $x = 0$ to 9×10^{-3} or 0.2 S· cm^{-1} (depending on crystallographic direction) for $x = 0.28$ in "nanobelt" (NB) samples. At the smallest lithium intercalation levels, electron mobilities were concluded to be governed by an adiabatic small polaron hopping mechanism in both samples, consistent with conclusions drawn from earlier studies of electron conductivity in pristine MoO_3.[17] With increasing values of x, the spectroscopy results of Berthumeyrie *et al.* suggest a transition from a dominant polaron mechanism to a bipolaron mechanism in the CP samples, which was not observed in the NB samples. The differences found between NB and CP samples were suggested to be due to an enhanced role of surface-related effects in the former.

To provide expanded insights into the electronic conduction mechanisms in Li-intercalated α-MoO_3, we present here the results of a computational study of the electronic structure and mobilities of electron small polarons and their interaction with Li interstitial ions. We employ both density-functional theory with Hubbard-U corrections (DFT+U)[18,19] and hybrid functional[20–22] methods to compute the orbital occupancies and atomic structural changes associated with small polaron formation, the activation energies for adiabatic polaron transfer, and the binding energies of electron small polarons to Li ions. The calculations demonstrate a pronounced anisotropy in polaron mobilities within and across the bilayer sheets that are characteristic of the α-MoO_3 crystal structure, and yield magnitudes for the binding energies with Li ions that vary depending on the intercalation site.

Methodology

The crystal structure of the α-MoO_3 compound is orthorhombic with space group *Pbnm*. As illustrated in Figure 1, the crystal structure is characterized by a stacking of bilayer sheets which interact through a combination of electrostatic and dispersion forces[23,24] across the so-called "van der Waals" gaps. The bilayers are composed of MoO_6 octahedra, which share vertices along the *a* direction and edges along the *c* direction. These octahedra are highly distorted, with Mo-O bond lengths ranging from approximately 1.6 Å for the terminal oxygen ions (d_{MoO1}) at the top and bottom of the bilayer sheets, to approximately 2.3 Å for the oxygen ions forming the shared edges (d^*_{MoO3}).[25,26]

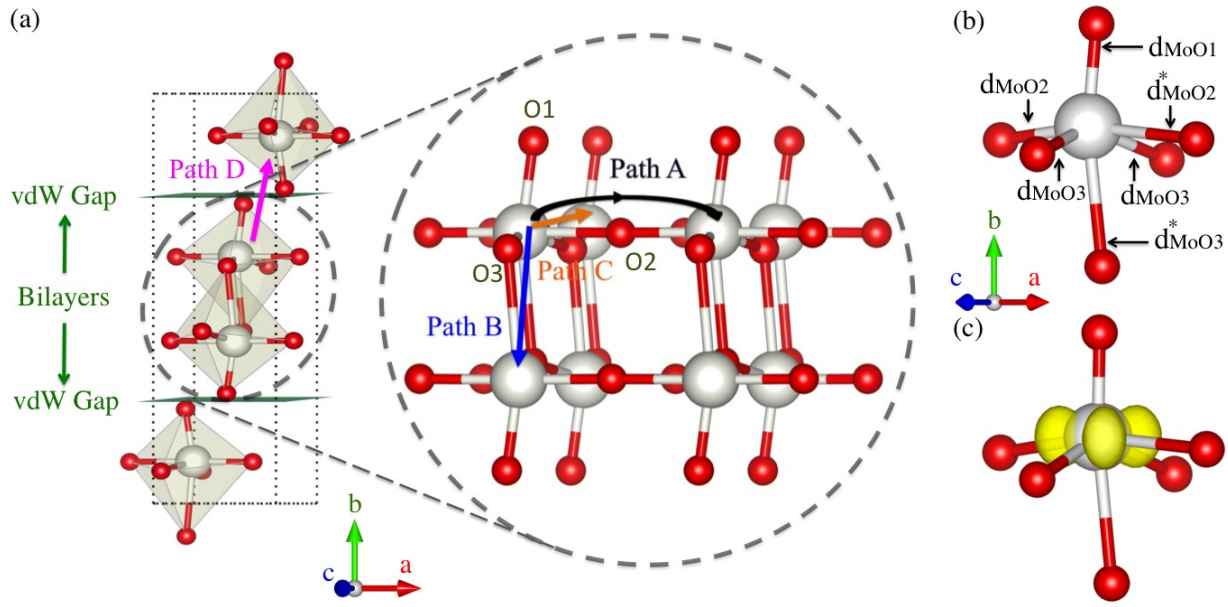

Figure 1: (a) The structure of α-MoO_3 and the local geometry of the MoO_6 octahedra within the bilayer sheets are illustrated in panels (a) and (b), respectively. Also shown in panel (a) are three polaron hopping directions within the bilayer sheets (paths A, B and C) and one path normal to the van der Waals gaps (path D). In panel (c) the geometry of a MoO_6 octahedron with a localized electron small polaron on the Mo ion is illustrated; the yellow isosurface corresponds to induced charge density due to the electron small polaron, plotted at a value of the electron density equal to 0.025 eÅ^{-3}.

The properties of localized electron small polarons in α-MoO_3 (see Figure 1(c)) are studied using both DFT+U and hybrid-functional methods. The DFT+U calculations are based on the

formalism of Dudarev *et al.*,[19] in which the total energy of the system is expressed as:

$$E^{\mathrm{DFT+U}} = E^{\mathrm{DFT}} + \frac{U_{\mathrm{eff}}}{2}\sum_{\sigma} Tr[\rho^{\sigma} - \rho^{\sigma}\rho^{\sigma}], \tag{1}$$

where E^{DFT} corresponds in this work to the DFT energy in the Perdew-Burke-Ernzerhof (PBE) generalized gradient approximation,[27,28] ρ^{σ} denotes the spin (σ) dependent on-site density matrix, and the parameter multiplying the last term on the right-hand side of Eq. (1) is defined as $\mathrm{U_{eff}} \equiv U - J$ in terms of the Hubbard-model U and J parameters. In the hybrid-functional calculations we employ the formalism developed by Heyd, Scuseria and Ernzerhof (HSE),[20–22] where the exchange-correlation energy (E_{xc}^{HSE06}) is formulated as:

$$E_{xc}^{\mathrm{HSE06}} = E_{x}^{\mathrm{DFT}}(\mu) + E_{c}^{\mathrm{DFT}} - \frac{1}{4}E_{x}^{\mathrm{DFT,SR}}(\mu) + \frac{1}{4}E_{x}^{\mathrm{HF,SR}}(\mu). \tag{2}$$

with E_{x}^{DFT} and E_{c}^{DFT} denote the exchange and correlation energies in DFT under the PBE-GGA. In this formalism 25% of the short-range part of the DFT exchange energy ($E_{x}^{\mathrm{DFT,SR}}(\mu)$) is replaced by the exact nonlocal Hartree-Fock exchange ($E_{x}^{\mathrm{HF,SR}}(\mu)$) evaluated with a short-range screened Coulomb kernel, where μ is an adjustable screening parameter determining the distance $2/\mu$ at which $E_{x}^{\mathrm{HF,SR}}$ becomes negligible. In this work, μ is set as 0.2 Å, which is the shortest screening distance recommended by Krukau *et al.*[29] for the HSE06 scheme.

The DFT+U and hybrid-functional calculations were performed within the formalism of the projector augmented wave (PAW) method,[30,31] as implemented in the Vienna ab-initio simulation package (VASP) code.[32–35] The electronic states were expanded in a plane-wave basis with a kinetic energy cutoff of 500 eV. Use was made of the PAW potentials designated "Mo" and "O" in the VASP library, corresponding to valence electron configurations of $4d^5 5s^1$ for molybdenum and $2s^2 2p^4$ for oxygen.

For the DFT+U calculations, all atomic coordinates were relaxed until the forces on the ions were converged to within 0.01 eV/Å, holding the lattice parameters fixed at the experimentally-measured values, while for the hybrid calculations all atomic positions were fixed at the values

obtained from the DFT+U relaxations. We note that previous work[24] has shown that in order to achieve good agreement with experimentally measured values of the *b* lattice constant in DFT-based calculations, it is necessary to account for van der waals corrections using, for example, the DFT-D2[36] or vdW-DF[37] approaches. In the present work such vdW corrections were not included and instead all lattice parameters were frozen at the experimentally measured values for pristine MoO_3. This approach leads to the introduction of strain energy associated with polaron formation and/or Li intercalation; however, the effects on the calculated bond lengths and hopping barriers reported below were investigated and found to be relatively small, on the order of 0.02 Å and 0.02 eV, respectively.

Electronic density-of-states (DOS) calculations were performed using the conventional unit cell, containing four formula units, with a $7 \times 5 \times 7$ k-point grid employed to sample the Brillouin zone. Calculations including polarons and intercalated Li ions made use of a $3 \times 1 \times 3$ supercell containing 36 formula units (108 ions). In the DFT+U supercell calculations, the Brillouin-zone sampling was performed using a $3 \times 3 \times 3$ k-point grid in combination with the Methfessel-Paxton scheme[38] and a smearing of 0.1 eV. For hybrid-functional calculations the same size supercells were employed, but with a single k-point (Γ) used to sample the Brillouin zone. Several tests were performed to estimate the convergence of the DFT+U results with respect to supercell size, plane-wave cutoff and k-point density; these tests indicate that the polaron migration energies and the changes in bond length associated with polaron defect formation are converged with respect to these parameters to within a precision of approximately 0.02 eV and 0.03 Å, respectively.

The present computational study focuses on electron small polarons that result from the occupation of one of the unoccupied 4*d* orbitals in the Mo^{6+} ion, to form a Mo^{5+} ion. In the calculations, small polarons are formed through the introduction of an extra electron in the computational cell (with charge-compensating positive background charge) or by explicit introduction of a Li atom. Since it is possible for the electron forming the polaron defect to occupy different 4*d* orbital states, we undertook a detailed investigation of the preferred occupancy using an occupation matrix control (OMC) approach.[39] The calculations established that the lowest-energy state for the

electron small polaron corresponds to the occupation of a d_{xz} orbital, as discussed below, and as illustrated in Fig. 1(c). The formation of this polaron defect leads to distortions of the bond lengths with neighboring oxygen ions, which is most pronounced for the bond with the corner-shared O2 ion (see Fig. 1(b)). Consequently, in studies of Li-ion binding we were able to control the position of the polaron relative to the Li ion by selectively perturbing the Mo-O2 bond lengths in the desired MoO_6 octahedron.

In the DFT+U calculations undertaken in this work, use was made of a value of U_{eff} = 6 eV. This value is similar to that derived by Coquet *et al.* (U_{eff} = 6.3 eV)[40] by comparing the results of periodic plane-wave DFT+U and wavefunction-based cluster calculations of oxygen defect formation on the (010) surface of α-MoO_3. The value of U_{eff} used here is, however, considerably smaller than that suggested by Lutfalla *et al.*[41] (8.6 eV) by fitting the experimental enthalpy for the hydrogen reduction reaction of MoO_3 to MoO_2: $MoO_3 + H_2 \rightarrow MoO_2 + H_2O$. We note that the values of U_{eff} used in this work and the study by Coquet *et al.* are both close to the value of $\approx$ 6.5 eV that we have found to give rise to the most linear variation in the energy as a function of the occupation of the Mo d_{xz} orbital (from zero to one electron); as discussed in Refs.,[42,43] a linear dependence of the energy on orbital occupation suggests a value of U_{eff} that maximally cancels the DFT self-interaction error. The degree of charge localization obtained with U_{eff} = 6 eV in the present DFT+U calculations is found to be quantitatively very similar to that obtained with the HSE06 method for the same atomic geometry. Specifically, the HSE06 calculation yields a charge difference of 1.02 electrons between a Mo^{5+} ion (occupied by an electron small polaron) and a Mo^{6+} ion (in pristine MoO_3) within a spherical integration volume with radius of 1.455 Å; the corresponding value obtained in the DFT+U calculations with U_{eff} = 6 eV is 1.01 electrons. Finally, we note that the calculated values for the polaron migration and Li-binding energies presented below showed relatively small changes (around 0.02 eV) resulting from increases in the value of U_{eff} in the range of 6 to 7 eV.

For calculations of the adiabatic polaron migration energies, we employed the approach proposed by Maxisch *et al.*[44] and Ong *et al.*[45] In this approach, energies are computed on the Born-

Oppenheimer surface, for a set of configurations with atomic coordinates ($\{q\}$) linearly interpolated between those corresponding to the initial and final states, $\{q_i\}$ and $\{q_f\}$, respectively:

$$\{q_x\} = (1-x)\{q_i\} + (x)\{q_f\}, \tag{3}$$

with x varying in the range from 0 to 1. For calculations of polaron migration energies away from intercalated Li ions, the initial and final states are equivalent by symmetry, such that the energy calculated for $x = 0.5$ in Eq. (3) provides the estimate of the migration energy barrier. A schematic illustration of the approach is given in Figure 2.

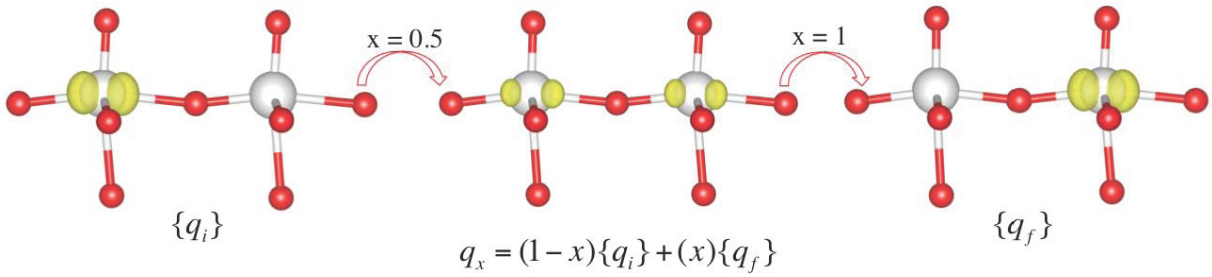

Figure 2: An illustration of the approach used to compute adiabatic polaron migrations energies from calculations on the Born-Oppenheimer surface for atomic coordinates linearly interpolated between those corresponding to polaron occupation on the left-most Mo ion and on the right-most Mo-ion. The atomic positions are taken from a calculation corresponding to polaron hopping along path A in Figure 1(a).

Results and Discussion

Atomic and Electronic Structure

Figure 3 shows calculated electronic density of states (DOS) for MoO_3 obtained in the present work using DFT+U and HSE06 methods. The results are qualitatively similar to each other and to previously published calculations .[23,40,46,47] The results feature a conduction band with predominantly Mo 4*d* character and a valence band with states having primarily O 2*p* character near the Fermi level, and states with significant hybridization between O *p* and Mo *d* states at higher

binding energies. Consistent with previous calculations, the value of the bandgap (E_g) of 2.09 eV computed by DFT+U is approximately ten percent larger than that derived by GGA-PBE calculations. The DFT+U calculations underestimate the experimentally measured band gap, which has been reported to be in the range of $E_g \approx$ 2.8-3.5 eV .[47–51] While the shape and character of the states for the HSE06-computed DOS are very similar to those obtained with the DFT+U method, the band gap has a significantly larger value of 2.84 eV, which is closer to experimental measurements. In addition, the HSE06 functional predicts a larger valence-band width than DFT+U: 6.5 eV versus 6.3 eV, respectively; the HSE06 value is in better agreement with but still smaller than the value of 6.98 eV derived from the X-ray photoemission data of Itoh *et al.*[48]

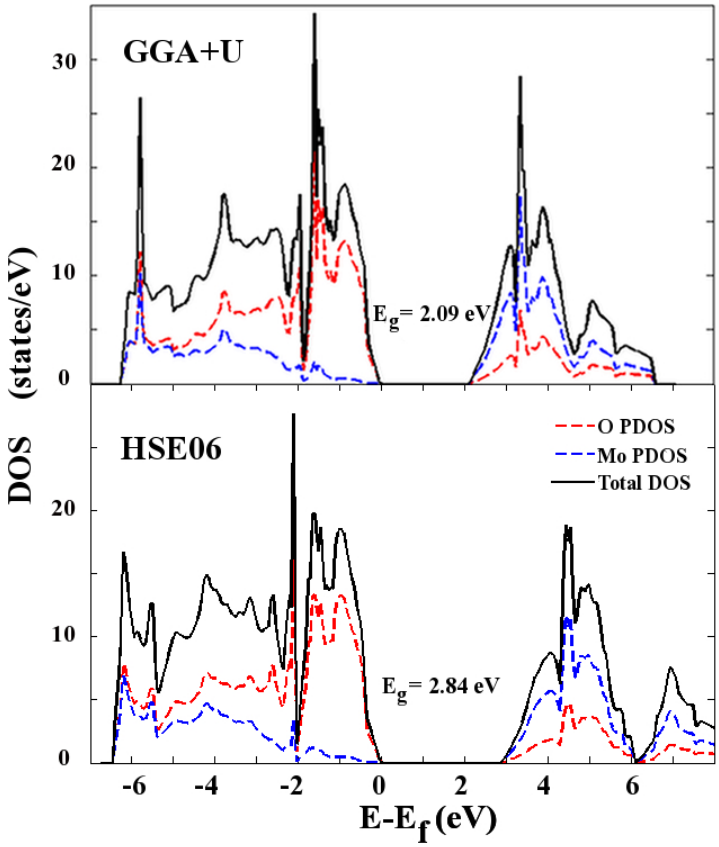

Figure 3: Comparison of projected density of states (per formula unit) of α-MoO_3 calculated by the DFT+U and HSE06 methods.

We consider next the electronic and atomic structure associated with the formation of the electron small polaron defect, which will be referred to as a Mo^{5+} ion in what follows. Figure 1(c)

shows the change in charge density associated with the formation of Mo^{5+} from the Mo^{6+} ion in bulk MoO_3. The shape of the added electron charge density is consistent with occupation in a state that has predominant $4d_{xz}$ character, as confirmed from an analysis of projected densities of states. From extensive tests performed with the occupation-matrix-control method referenced in the previous section, it was verified that occupancy of the $4d_{xz}$ orbital leads to the lowest energy for the Mo^{5+} ion in this structure. The defect state associated with this polaron defect is found to be highly localized; in the DFT+U calculations with U_{eff} = 6 eV this state sits at an energy approximately 1.5 eV below the conduction-band edge. The location of this defect state in the bandgap is found to be somewhat sensitive to the value of U_{eff} employed in the DFT+U calculations; the defect band moves approximately 0.2 eV lower (higher) in energy when U_{eff} increases (decreases) from 6 eV to 7 eV (5 eV).

Previous DFT and crystal field theory calculations have demonstrated that the ordering of the *d*-orbital energy levels for Mo^{5+} in the MoO_3 structure is highly sensitive to the nature of the structural distortions associated with the octahedral arrangement of the oxygen ions around the cation.[52] It is thus of interest to analyze the nature of the bonding environment before and after the introduction of the polaron defect, as summarized in Table 1. In bulk α-MoO_3, there exist three symmetry-distinct oxygen-ion positions, labeled as O1, O2 and O3 in Figure 1(a), following the notation introduced by Corà *et al.*[23] As a consequence, there are five different types of bonds in a given MoO_6 octahedron, labeled as: d_{MoO1}, d_{MoO2}, d^*_{MoO2}, d_{MoO3} and d^*_{MoO3}, respectively (see Figure 1(c)). As shown in Table 1, the bonding for a bulk Mo^{6+} ion in MoO_3 is characterized by the formation of a relatively short bond with the terminal oxygen (O1), and relatively long bonds to two of the O2 and O3 ions. The calculated results obtained with DFT+U in the present work for the distribution of bond lengths surrounding the Mo^{6+} ion in MoO_3 are shown in Table 1 to be in good agreement with experimental measurements[53,54] and previous calculations.[24] The second column of Table 1 lists the bond lengths surrounding the polaron on the Mo^{5+} ion. A comparison with the results for Mo^{6+} shows that the main effect of polaron formation is to extend the length of the Mo-O2 (d_{MoO2}) bond, by approximately 0.2 Å, presumably due to the electrostatic repulsion

between the charge in the d_{xz} orbital and the nearest-neighbor O2 ion in the *a*-*c* plane.

Table 1: DFT+U calculated Mo-O bond lengths (in units of Å) for Mo^{5+} and Mo^{6+} sites in α-MoO_3 are listed and compared with values reported in previous publications.

	Polaron site (Mo^{5+})	Nonpolaron site (Mo^{6+})			
	This work	This work	DFT-D2[24]	Exp[53]	Exp[54]
d_{MoO1}	1.67	1.69	1.70	1.68	1.63
d_{MoO2}	1.97	1.78	1.77	1.74	1.74
d^{*}_{MoO2}	2.20	2.21	2.19	2.25	2.24
d_{MoO3}	2.01	1.96	1.95	1.95	1.96
d^{*}_{MoO3}	2.40	2.38	2.40	2.31	2.30

Polaron Migration

In Figure 1(a) we label four distinct paths for a polaron hopping to neighboring Mo sites. Path A involves a hop along the *a* crystallographic direction, to the nearest-neighbor Mo site within the same *a*-*c* plane in the bilayer sheet; the Mo ions on each side of this path are linked by a corner-shared oxygen ion, and are separated by a jump distance of 3.96 Å. Path C also connects two Mo ions within the same *a*-*c* plane that are linked by corner-shared oxygen ions, and involves a hop along the *c* direction by a shorter distance of 3.70 Å. Path B connects two Mo ions in different *a*-*c* planes within the bilayer sheets that are linked across the shared edge of neighboring octahedra; this path involves the shortest hop distance of 3.39 Å. We note that path B has been referred to in the literature as a “zig-zag" path[16] as it involves motion along the direction *c* and up and down along *b* direction within the bilayer sheet. Finally, path D involves polaron migration across the van der Waals gap along the *b* direction, with the largest hop distance of 4.96 Å.

Figure 4 shows the calculated energies along the migration paths defined by Eq. (3) for each of the four jumps described above. The energy versus the reaction coordinate *x* obtained from the DFT+U calculations is plotted with solid symbols connected by lines. The energy at the binding and saddle point sites are also computed by hybrid functionals, with results shown by open symbols. Comparing first the different calculated results, it can be seen that the HSE06 activation energies are consistently lower than those obtained by DFT+U, by up to 15 % in magnitude. A

fraction of this difference originates from the different k-point sampling used in the DFT+U and HSE06 calculations. When the k-point grid for the DFT+U method is changed from $3 \times 1 \times 3$ to $1 \times 1 \times 1$ (as used in the HSE06 calculations), the calculated activation energy along path A is calculated to decrease by 0.02 eV; the remainder of the 0.06 eV difference between HSE06 and DFT+U results shown in Figure 4 can thus be attributed to the different functionals.

A major feature of the results shown in Figure 4 is the high anisotropy in the activation energies along the different crystallographic directions, and it is important to note that the relative ordering of the activation energies for these different paths is predicted to be the same by both DFT+U and HSE06 methods. The calculated results give the lowest energy barrier for hopping along path A, in the *a* crystallographic direction. The next lowest-energy hop is along path C, along the crystallographic *c* direction. Thus, polaron migration is predicted to be fastest between Mo ions that lie within the same plane of the bilayer sheet, which are all linked by corner-shared oxygen ions. Contrary to assumptions in the literature, the path involving the shortest jump distance, namely the zig-zag path B, involves a significantly higher activation energy (by 0.1 to 0.2 eV) than migration along either paths A or C. The results thus suggest that the presence of a corner-shared oxygen ion significantly facilitates polaron migration, despite the larger jump distances for paths A and C relative to B.

The highest anisotropy is found between the low-energy jumps along the *a* and *c* crystallographic directions within the bilayer sheets, and hopping along path D, across the van der Waals gaps. With the calculated polaron hopping barriers labeled in Figure 4, we can roughly estimate the anisotropy of polaron mobilities within and across the bilayer sheets using the expression for the hop frequency $\nu = \nu^* \exp(-\Delta E/k_B T)$, assuming that the attempt frequency ν^* varies relatively weakly amongst the different paths. With this assumption, the room temperature mobility parallel to the bilayer sheets is predicted to be approximately five orders of magnitude faster than that normal, due to the high activation energy for hopping across the van der Waals gaps. These estimates are in reasonable agreement with experimental measurements that report room-temperature electron conductivities of 10^{-10} and 10^{-4} S$\cdot$ cm^{-1} perpendicular to and within the MoO_3 bilayer

sheets, respectively.[3,55] It is also worth noting that Berthumeyrie *et al.*[16] report a measured polaron hopping activation energy of 0.43 eV in “classical particle" samples. Considering that the measurements on these samples are likely to represent an average over crystallographic orientations, a direct comparison with the present results is difficult. However, the value of 0.43 eV does lie within the range of computed values for the polaron hopping barriers reported in Figure 4.

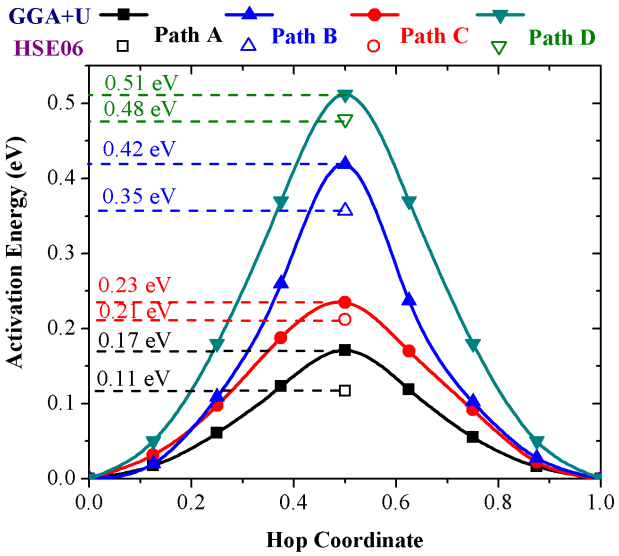

Figure 4: Polaron migration energies calculated with DFT+U (filled) and HSE06 (unfilled) methods along the different migration paths in α-MoO_3 illustrated in Figure 1.

Lithium-Polaron Interactions

To investigate the interaction energies between intercalated Li ions and electron small polarons, we extended the DFT+U calculations described above, through the incorporation of single Li atoms directly in the $3 \times 1 \times 3$ supercells, giving an overall composition of $Li_{0.028}MoO_3$. Two intercalation sites were considered for the Li ions in these calculations, as illustrated in Figure 5. One site is located within the two-dimensional van der Waals gaps within the α-MoO_3 structure, and will be referred to in what follows as an interlayer position. The second is located within one-dimensional channels and will be referred to as the intralayer position. When Li atoms are positioned in either site, and a neighboring MoO_6 octahedron is distorted to facilitate polaron formation, the calcula-

tions converge to a state in which the valence electron from Li is transferred to the targeted Mo^{6+} site, leading to the formation of Li^{+} and Mo^{5+} ions.

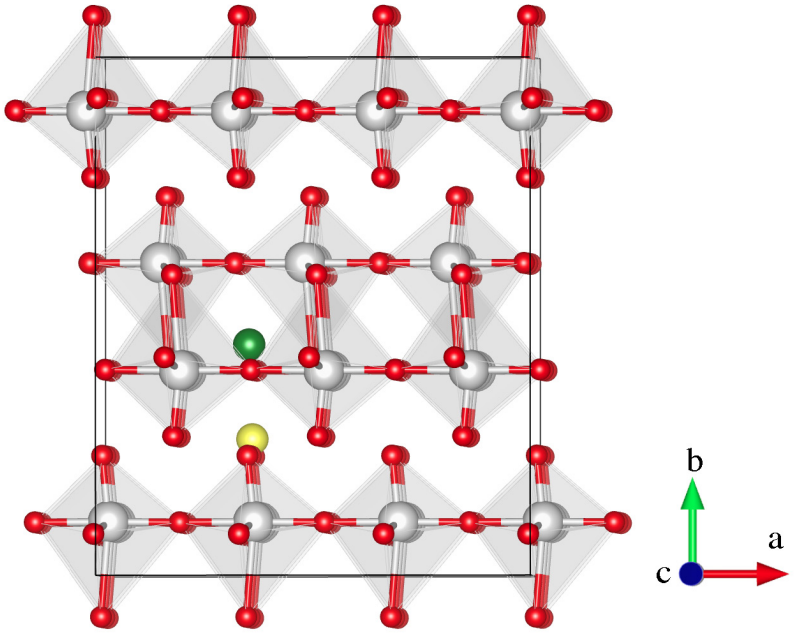

Figure 5: Lithium intercalation sites in a α-MoO_3 supercell. The yellow sphere denotes the interlayer site within the interlayer van der Waals gap, and the green sphere denotes the intralayer site within the one-dimensional channels formed between MoO_6 octahedron within the bilayer sheets.

When the Mo^{5+} polaron is located as a nearest neighbor to the intercalated Li^{+} ion, the DFT+U calculations predict that the intralayer site is slightly lower in energy, by approximately 0.05 eV. However, this result is influenced by the relative magnitudes of the binding energy between Li^{+} and Mo^{5+} ions in the two sites. Specifically, by comparing the energy differences between states in which the polaron is nearest and furthest from a Li^{+} ion in each site, we derive estimates of the binding energy E_b given in Table 2. It can be seen that the binding between the polaron and Li^{+} ion is stronger for the intralayer site by approximately 0.08 eV. The larger binding energy in the intralayer site correlates with the shorter distance between Li^{+} and Mo^{5+} ions in this site (2.79 Å) versus the interlayer site (4.69 Å). As a consequence of the different values for the binding energies, if the polaron is completely dissociated from the intercalated Li^{+} ion, the site stability reverses, with the interlayer site being weakly favored. Overall, these results suggest that site selection of intercalated Li^{+} ions is governed by competing thermodynamic effects that balance

configurational entropy (enhanced by dissociation of Li ions from polarons[56]) and binding energies (favoring association of Li ions and polarons). It is worth noting that despite the slightly higher Li-ion concentration used in our supercell calculations (0.028 Li to Mo fraction), the magnitude of the Li-polaron binding energies computed by DFT+U are in reasonable agreement with the estimate of 0.22 eV derived from dielectric spectroscopy measurements on $Li_{0.01}MoO_3$ samples by Berthumeyrie *et al.*[16]

Table 2: Calculated migration barriers (E_m) for electron small polarons bound to neighboring Li^+ ions, and binding energies (E_b) between polarons and Li^+ ions, as obtained by the DFT+U method in $3 \times 1 \times 3$ supercells with composition $Li_{0.028}MoO_3$. Calculated results are compared with experimental measurements reported for $Li_{0.01}MoO_3$. All energies are reported in units of eV.

Intercalation Site	E_m		E_b	
	Path A	Path C	Cal.	Exp.[16]
Interlayer	0.23	0.29	0.26	0.22
Intralayer	0.27	0.34	0.34	

Also listed in Table 2 are results obtained by DFT+U for the activation energies for hopping of a polaron away from the nearest neighbor of a Li^+ ion along the low-energy paths A and C. From a comparison of the results in Table 2 with those plotted in Figure 4, it can be seen that the migration energy of polarons bound to Li ions in the interlayer site increases by approximately 0.06 eV. A slightly larger increase is found for polarons bound to Li ions in interlayer sites, where migration energies along both paths A and C are raised by approximately 0.1 ev.

Summary

The properties of electron small polarons in α-MoO_3 have been investigated computationally using both DFT+U and hybrid-functional HSE06 methods. The calculations establish that the small polaron forms in an electronic state that has predominantly Mo $4d_{xz}$ character. Polaron formation gives rise to a pronounced elongation in the nearest-neighbor corner-shared oxygen ion within the *a*-*c* plane. The adiabatic barriers for polaron hopping in α-MoO_3 are calculated by DFT+U to be 0.17 eV and 0.23 eV for hopping within the same *a*-*c* plane within the bilayer sheets along the *a*

and *c* crystallographic directions, respectively. Hopping between the nearest-neighbor Mo ions, along the zig-zag chains within the bilayers is calculated to involve a significantly larger hopping barrier of 0.42 eV. The largest barrier for polaron transport is calculated to be 0.51 eV, for hopping across the van der Waals gap, along the *b* direction. HSE06 calculations yield slightly smaller activation energies relative to DFT+U, but with very similar anisotropies. Overall the calculated results suggest a high degree of anisotropy in the polaron mobilities, consistent with experimental measurements.

The binding energy of polarons to intercalated Li ions is calculated by DFT+U to be 0.34 eV and 0.26 eV in $Li_{0.028}MoO_3$ supercells, when Li resides within the one-dimension interlayer channel positions or within the two-dimensional van der Waals gaps, respectively. The higher binding energy favors intercalation of Li into the interlayer positions when they are bound to a polaron, while the interlayer position is favored when the Li ion and polaron are dissociated. Polaron-Li binding is also calculated to give rise to an increase in the activation energy for polaron hopping by approximately 0.1 eV.

Acknowledgements

The work of VO, HL and MA, as well as most computational work by HD, were supported as part of the Molecularly Engineered Energy Materials (MEEM), an Energy Frontier Research Center funded by the U.S. Department of Energy (DOE), Office of Science, Office of Basic Energy Sciences under Award Number DE-SC0001342. The work of BS and FZ, and the initial work of HD related to the HSE06 calculations, was performed under the auspices of the U.S. DOE by Lawrence Livermore National Laboratory under Contract DE-AC52-07NA27344. This research used resources of the National Energy Research Scientific Computing Center, which is supported by the Office of Science of the U.S. DOE under Contract No. DE-AC02-05CH11231.

References

[1] Zhou, J.; Deng, S.; Xu, N.; Chen, J.; She, J. *Applied physics letters* **2003**, *83*, 2653–2655.

[2] Li, G.; Jiang, L.; Pang, S.; Peng, H.; Zhang, Z. *The Journal of Physical Chemistry B* **2006**, *110*, 24472–24475.

[3] Mai, L.; Hu, B.; Chen, W.; Qi, Y.; Lao, C.; Yang, R.; Dai, Y.; Wang, Z. *Advanced Materials* **2007**, *19*, 3712–3716.

[4] Lee, S.-H.; Kim, Y.-H.; Deshpande, R.; Parilla, P. A.; Whitney, E.; Gillaspie, D. T.; Jones, K. M.; Mahan, A.; Zhang, S.; Dillon, A. C. *Advanced Materials* **2008**, *20*, 3627–3632.

[5] Yan, B.; Zheng, Z.; Zhang, J.; Gong, H.; Shen, Z.; Huang, W.; Yu, T. *The Journal of Physical Chemistry C* **2009**, *113*, 20259–20263.

[6] Brezesinski, T.; Wang, J.; Tolbert, S.; Dunn, B. *Nature materials* **2010**, *9*, 146–151.

[7] Liang, R.; Cao, H.; Qian, D. *Chemical Communications* **2011**, *47*, 10305–10307.

[8] Rozzi, C.; Manghi, F.; Parmigiani, F. *Physical Review B* **2003**, *68*, 075106.

[9] Lin, C.-T.; Yeh, C.-H.; Chen, M.-H.; Hsu, S.-H.; Wu, C.-I.; Pi, T.-W. *Journal of Applied Physics* **2010**, *107*, 053703–053703.

[10] Hu, X. K.; Qian, Y. T.; Song, Z.; Huang, J. R.; Cao, R.; Xiao, J. Q. *Chemistry of materials* **2008**, *20*, 1527–1533.

[11] Hu, Z.; Zhou, C.; Zheng, M.; Lu, J.; Varghese, B.; Cheng, H.; Sow, C.-H. *The Journal of Physical Chemistry C* **2012**, *116*, 3962–3967.

[12] Hassan, M. F.; Guo, Z.; Chen, Z.; Liu, H. K. *Journal of Power Sources* **2010**, *195*, 2372–2376.

[13] Xue, X.-Y.; Chen, Z.-H.; Xing, L.-L.; Yuan, S.; Chen, Y.-J. *Chemical Communications* **2011**, *47*, 5205–5207.

[14] Pandit, A.; Prasad, M.; Ansari, T.; Singh, R.; Wanklyn, B. *Solid State Communications* **1991**, *80*, 125 – 127.

[15] Julien, C.; Khelfa, A.; Hussain, O.; Nazri, G. *Journal of Crystal Growth* **1995**, *156*, 235 – 244.

[16] Berthumeyrie, S.; Badot, J.-C.; Pereira-Ramos, J.-P.; Dubrunfaut, O.; Bach, S.; Vermaut, P. *The Journal of Physical Chemistry C* **2010**, *114*, 19803–19814.

[17] Navas, I.; Vinodkumar, R.; Lethy, K.; Detty, A.; Ganesan, V.; Sathe, V.; Pillai, V. *Journal of Physics D: Applied Physics* **2009**, *42*, 175305.

[18] Anisimov, V. I.; Zaanen, J.; Andersen, O. K. *Phys. Rev. B* **1991**, *44*, 943–954.

[19] Dudarev, S. L.; Botton, G. A.; Savrasov, S. Y.; Humphreys, C. J.; Sutton, A. P. *Phys. Rev. B* **1998**, *57*, 1505–1509.

[20] Heyd, J.; Scuseria, G. E.; Ernzerhof, M. *The Journal of Chemical Physics* **2003**, *118*, 8207–8215.

[21] Heyd, J.; Scuseria, G. E. *The Journal of Chemical Physics* **2004**, *121*, 1187–1192.

[22] Heyd, J.; Scuseria, G. E.; Ernzerhof, M. *The Journal of Chemical Physics* **2006**, *124*, 219906.

[23] Corà, F.; Patel, A.; Harrison, N. M.; Roetti, C.; Catlow, C. R. A. *Journal of Materials Chemistry* **1997**, *7*, 959–967.

[24] Ding, H.; Ray, K. G.; Ozolins, V.; Asta, M. *Phys. Rev. B* **2012**, *85*, 012104.

[25] Sitepu, H. *Powder Diffraction* **2009**, *24*, 315–326.

[26] Negishi, H.; Negishi, S.; Kuroiwa, Y.; Sato, N.; Aoyagi, S. *Physical Review B* **2004**, *69*, 064111.

[27] Perdew, J. P.; Burke, K.; Ernzerhof, M. *Phys. Rev. Lett.* **1996**, *77*, 3865.

[28] Perdew, J. P.; Burke, K.; Ernzerhof, M. *Phys. Rev. Lett.* **1997**, *78*, 1396.

[29] Krukau, A. V.; Vydrov, O. A.; Izmaylov, A. F.; Scuseria, G. E. *The Journal of Chemical Physics* **2006**, *125*, 224106.

[30] Blöchl, P. E. *Phys. Rev. B* **1994**, *50*, 17953.

[31] Kresse, G.; Joubert, D. *Phys. Rev. B* **1999**, *59*, 1758.

[32] Kresse, G.; Hafner, J. *Phys. Rev. B* **1993**, *47*, 558.

[33] Kresse, G.; Hafner, J. *Phys. Rev. B* **1994**, *49*, 14251.

[34] Kresse, G.; Furthmüller, J. *Comput. Mat. Sci.* **1996**, *6*, 15.

[35] Kresse, G.; Furthmüller, J. *Phys. Rev. B* **1996**, *54*, 11169.

[36] Grimme, S. *Journal of computational chemistry* **2006**, *27*, 1787–1799.

[37] Klimeš, J.; Bowler, D. R.; Michaelides, A. *Journal of Physics: Condensed Matter* **2010**, *22*, 022201.

[38] Methfessel, M.; Paxton, A. T. *Phys. Rev. B* **1989**, *40*, 3616–3621.

[39] Zhou, F.; Ozoliņš, V. *Physical Review B* **2009**, *80*, 125127.

[40] Coquet, R.; Willock, D. *Phys. Chem. Chem. Phys.* **2005**, *7*, 3819–3828.

[41] Lutfalla, S.; Shapovalov, V.; Bell, A. T. *Journal of Chemical Theory and Computation* **2011**, *7*, 2218–2223.

[42] Lany, S.; Zunger, A. *Physical Review B* **2009**, *80*, 085202.

[43] Erhart, P.; Klein, A.; Åberg, D.; Sadigh, B. *arXiv preprint arXiv:1402.0435* **2014**,

[44] Maxisch, T.; Zhou, F.; Ceder, G. *Phys. Rev. B* **2006**, *73*, 104301.

[45] Ong, S. P.; Chevrier, V. L.; Ceder, G. *Phys. Rev. B* **2011**, *83*, 075112.

[46] Sayede, A.; Amriou, T.; Pernisek, M.; Khelifa, B.; Mathieu, C. *Chemical physics* **2005**, *316*, 72–82.

[47] Scanlon, D. O.; Watson, G. W.; Payne, D. J.; Atkinson, G. R.; Egdell, R. G.; Law, D. S. L. *The Journal of Physical Chemistry C* **2010**, *114*, 4636–4645.

[48] Itoh, M.; Hayakawa, K.; Oishi, S. *Journal of Physics: Condensed Matter* **2001**, *13*, 6853.

[49] Irfan,; Ding, H.; Gao, Y.; Kim, D. Y.; Subbiah, J.; So, F. *Applied Physics Letters* **2010**, *96*, 073304.

[50] Hu, B.; Mai, L.; Chen, W.; Yang, F. *ACS nano* **2009**, *3*, 478–482.

[51] Pandit, A.; Prasad, M.; Ansari, T.; Singh, R.; Wanklyn, B. *Solid state communications* **1991**, *80*, 125–127.

[52] Labanowska, M. *ChemPhysChem* **2001**, *2*, 712–731.

[53] Sitepu, H. *Powder Diffraction* **2009**, *24*, 315–326.

[54] Negishi, H.; Negishi, S.; Kuroiwa, Y.; Sato, N.; Aoyagi, S. *Phys. Rev. B* **2004**, *69*, 064111.

[55] Julien, C.; Nazri, G. *Solid State Ionics* **1994**, *68*, 111–116.

[56] Zhou, F.; Maxisch, T.; Ceder, G. *Physical review letters* **2006**, *97*, 155704.